Solution structure of robustoxin, the lethal neurotoxin from the funnel-web spider *Atrax robustus*

Paul K. Pallaghy[a], Dianne Alewood[b], Paul F. Alewood[b], Raymond S. Norton[a,*]

[a] *Biomolecular Research Institute, 343 Royal Parade, Parkville, Vic. 3052, Australia*
[b] *Centre for Drug Design and Development, University of Queensland, Brisbane, Qld. 4072, Australia*

Received 16 September 1997; revised version received 30 October 1997

Abstract The solution structure of robustoxin, the lethal neurotoxin from the Sydney funnel-web spider *Atrax robustus*, has been determined from 2D ^{1}H NMR data. Robustoxin is a polypeptide of 42 residues cross-linked by four disulphide bonds, the connectivities of which were determined from NMR data and trial structure calculations to be 1–15, 8–20, 14–31 and 16–42 (a 1–4/2–6/3–7/5–8 pattern). The structure consists of a small three-stranded, anti-parallel β-sheet and a series of interlocking γ-turns at the C-terminus. It also contains a cystine knot, thus placing it in the inhibitor cystine knot motif family of structures, which includes the ω-conotoxins and a number of plant and animal toxins and protease inhibitors. Robustoxin contains three distinct charged patches on its surface, and an extended loop that includes several aromatic and non-polar residues. Both of these structural features may play a role in its binding to the voltage-gated sodium channel.

Key words: Neurotoxic polypeptide (robustoxin); Nuclear magnetic resonance spectroscopy; Structure; Cystine knot; Beta-sheet; Funnel-web spider

1. Introduction

Funnel-web spiders belonging to the Mygalomorph family are found in many parts of Australia, with more than 30 species having been identified to date. One of these, the Sydney funnel-web spider *Atrax robustus*, has attracted considerable attention as it has been responsible for at least 14 human fatalities since 1927 [1]. Only the male *A. robustus* spider is capable of inflicting a lethal bite [2], and the venom has a remarkable species specificity, with newborn mice [3] and primates [4] being susceptible but most other species being unaffected [1,5]. Envenomation is associated with local pain, salivation, lachrymation, skeletal muscle fasciculation and disturbances in respiration, blood pressure and heart rate, followed by severe hypotension or death due to respiratory and circulatory failure [4,5]. The introduction of an effective antivenom in 1980 [6] has largely eliminated the public health risk of *A. robustus* envenomation, but there has been considerable interest in characterising the toxic components of the venom.

*Corresponding author. Fax: (61) (3) 9903 9655.
E-mail: ray.norton@molsci.csiro.au

Abbreviations: RBX, robustoxin from *Atrax robustus*; DQF-COSY, double quantum filtered 2D correlated spectroscopy; E-COSY, exclusive correlation spectroscopy; NOE, nuclear Overhauser enhancement; NOESY, 2D nuclear Overhauser enhancement spectroscopy; RMSD, root mean square difference; TOCSY, 2D total correlation spectroscopy

The polypeptide neurotoxin responsible for the major symptoms of envenomation was isolated from the venom of male *A. robustus* in 1983 [3]. This polypeptide, designated robustoxin (RBX), consists of a single chain of 42 amino acid residues, cross-linked by four disulphides. Its amino acid sequence has been determined [7] but the disulphide pairings have not been determined chemically, partly because of the difficulties engendered by a characteristic triplet of half-cystines at positions 14–16. The N- and C-termini, both of which are half-cystines, are unblocked. The production of significant amounts of toxin by synthetic or recombinant means has been hampered by the presence of four disulphides, and as a result the structure and structure-function relationships of this toxin have not been characterised.

Some progress has been made in defining its site of action in target tissues, which appears to be the voltage-gated sodium channel [8]. Indeed, there are some similarities between the effects of versutoxin, a homologue of RBX from a related funnel-web spider, on the gating and kinetics of the tetrodotoxin-sensitive sodium channel and those of sea anemone toxins [9] and scorpion α-toxins [10]. Assuming that this is the major site of action of RBX in vivo, a number of comparative studies with the anemone and scorpion toxins are required to determine the unique features of RBX action at the cellular level. Comparisons are also called for at the molecular level, in terms of both the binding site on the sodium channel and the structure and channel-binding surface of the toxin. The three-dimensional structure of RBX presented in this paper provides the necessary molecular basis for these comparisons.

2. Materials and methods

2.1. Materials

RBX was purified from crude male *A. robustus* venom by preparative reversed-phase HPLC on a Vydac C18 300 Å column (30 cm × 2.2 cm) using a linear gradient of 0–80% B at 1 ml/min over 60 min, where buffer A was 0.1% aqueous TFA and buffer B was 90% aqueous acetonitrile/0.1% TFA. ^2H_2O, NaO^2H and ^2HCl were obtained from Cambridge Isotope Laboratories (Andover, MA). Samples for NMR contained ca 1.3 mM RBX in either 90% H_2O/10% ^2H_2O or ^2H_2O at pH 5.0.

2.2. NMR spectroscopy

^{1}H NMR spectra were recorded on Bruker DRX-600 or AMX-500 spectrometers using 5-mm OD sample tubes. Except as otherwise noted, all experiments were carried out at 3°C. All two-dimensional (2D) spectra were recorded in phase-sensitive mode using the time-proportional phase incrementation method [11]. Water suppression was achieved using either low power presaturation or pulsed field gradients with the WATERGATE scheme and a 3-9-19 selective pulse [12].

2D homonuclear NOESY spectra [13,14] were recorded with mixing times of 50 and 250 ms. TOCSY spectra [15] were recorded using the DIPSI-2 spin-lock sequence [16] with spin-lock times of 40–70 ms. DQF-COSY [17] and E-COSY [18] spectra were also recorded. Typ-

PII S0014-5793(97)01452-X

ically, spectra were acquired with 400–500 t_1 increments, 128–224 scans per increment, 4096 data points and a relaxation delay of 1.8 s. The ^{1}H sweep width was 7374.6 Hz at 600 MHz. Spectra were processed using XWIN-NMR, version 1.3 (Bruker), and analysed using FELIX, version 95.0 (Molecular Simulations, San Diego, CA). Sine-squared window functions, phase shifted by 60–90°, were applied in both dimensions prior to Fourier transformation.

The $^3J_{NHC\alpha H}$ coupling constants were measured from a DQF-COSY spectrum. The appropriate rows were extracted from the spectrum, inverse Fourier transformed, zero-filled to 32 K, and multiplied by a Gaussian window function prior to Fourier transformation. $^3J_{C\alpha HC\beta H}$ coupling constants were measured from an E-COSY spectrum. Slowly exchanging amide protons were identified by dissolving the lyophilised protein in ^2H_2O at pH 5.0 and 5°C and recording a series of 1D and TOCSY spectra immediately after dissolution and over the next 9 h.

2.3. Structural constraints

Resonance assignments for RBX and aspects of its pH and temperature dependence will be reported elsewhere (M.D. Temple et al., to be published). NOESY cross-peak volumes measured from a 250-ms mixing time spectrum were used to calculate upper bound distance restraints. Peaks from the upper side of the diagonal were used except where peaks from the lower side were better resolved. Peak volumes were calibrated using an average of the volumes of four well-resolved geminal $C^\beta H$ cross-peaks. Distance constraints were calculated using volumes proportional to r^{-6} and pseudoatom corrections added where necessary. A 1.0 Å correction was then added to all distance constraints to allow for conformational averaging, errors in volume integration and the effects of spin diffusion (which are likely to be more significant at the low temperature used here). The final constraint set consisted of 110 intra-residue, 90 sequential, 42 medium-range ($1 < |i-j| \leq 4$) and 78 long-range NOEs, as well as 5 lower bound constraints based on the absence of NOEs [19].

Backbone dihedral angle constraints were inferred from $^3J_{NHC\alpha H}$ values as follows: $^3J_{NHC\alpha H} < 5$ Hz, $\phi = -60° \pm 30°$; $^3J_{NHC\alpha H} > 8$ Hz, $\phi = -120° \pm 40°$. Where possible, $^3J_{C\alpha HC\beta H}$ coupling constants were measured from passive couplings as displacements in E-COSY spectra or peak splittings in DQF-COSY spectra. The relative intensities of intra-residue $d_{\alpha\beta}(i,i)$ and $d_{N\beta}(i,i)$ NOEs were measured in 50-ms mixing time NOESY spectra. These $^3J_{C\alpha HC\beta H}$ coupling constants and NOE intensities were used to determine if side chains could be placed in one of the three staggered side-chain rotamer conformations ($\chi^1 = -60°$, 60°, or 180°), and to make stereospecific assignments. Stereospecific assignments of Asn and Gln side-chain amide protons were made on the basis of side-chain amide to methylene cross-peak intensities [20].

2.4. Structure calculations

Initial structures were generated with the distance geometry program DYANA, version 1.4 [21]. Several rounds of structure calculation were carried out using DYANA to resolve violated distance constraints and determine possible assignments for ambiguous NOE cross-peaks. This process was repeated until all the distance and angle restraints produced a set of structures that had no NOE distance violations > 0.3 Å or dihedral angle violations $> 5°$. Once the final set of restraints had been obtained, a new family of structures was generated using DYANA, and the 50 structures with the lowest penalty functions were refined in X-PLOR [22] using simulated annealing and energy minimisation, as described previously [23] but without neutralisation of charged side chains. The 20 best structures, on the basis of their stereochemical energies (i.e. excluding the electrostatic term), were chosen for structural analysis. These structures and the NMR restraints on which they were based have been submitted to the Protein Data Bank (accession no. 1QDP).

Structures were analysed using Insight II (Molecular Simulations) and PROCHECK_NMR [24]. Hydrogen bonds were identified in Insight II using a maximum C-N distance of 2.5 Å and a maximum angular deviation of 60° from linearity.

3. Results

3.1. Temperature

Attempts to obtain a complete set of resonance assignments from spectra recorded at pH 5.0 and ambient temperatures failed because of the absence of 2D connectivities to a number of backbone amide protons. Reducing the pH to 3.5 did not ameliorate this problem, but lowering the temperature did. This is illustrated in Fig. 1, where sharpening of the amide resonances of Arg^5 and Glu^{12} relative to surrounding NH resonances is evident as the temperature was reduced from 15°C (Fig. 1A) to 3°C (Fig. 1B). There were several backbone amide resonances which did not give observable cross-peaks at 15°C but did at 3°C, and there were some (notably residues 24–26) that gave only very weak cross-peaks even at 3°C. As residues 24–26 lie in an Ω-loop that is not well defined in the structure (see below), it is likely that conformational averaging is one contributor to this broadening. For this reason the structure calculations were based on NMR data recorded at 3°C. Comparison of well-resolved aliphatic and aromatic resonances at 3°C with those at ambient temperatures showed that their chemical shifts were essentially invariant over this temperature range, the only effect being a sharpening of the CH resonances at higher temperatures (as expected, and in contrast to the behaviour of several backbone amide resonances).

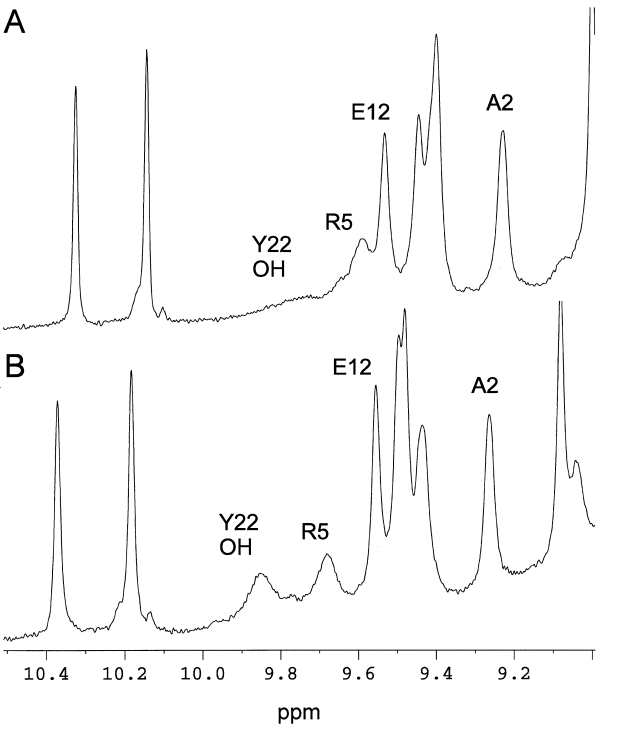

Fig. 1. Downfield regions of 1D spectra of RBX in 90% H_2O/10% ^2H_2O at pH 5.0 and 3°C (A) or 15°C (B). Note that the backbone amide resonances of Arg^5 and Glu^{12} are broader relative to the two indole NH resonances at 10.2–10.4 ppm at the higher temperature, whereas many amide and CH resonances became sharper (as expected). The backbone amide resonances of residues 24–26 (not shown here) were still broad and gave very weak 2D cross-peaks even at 3°C.

3.2. Determination of disulphide pairings

Structure calculations were carried out in DYANA using the final set of distance and angle restraints, but with the half-cystine residues left unconnected. The S–S and C^β–C^β distances among all half-cystine residues in the resulting structures were analysed to determine the correct disulphide pairings. From this analysis the C1–C15, C14–C31 and C16–C42 con-

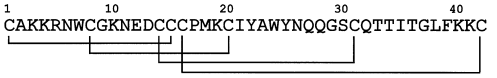

Fig. 2. Amino acid sequence of RBX [7], showing the disulphide connectivities determined from NMR data.

nectivities were defined unequivocally, leaving C8–C20 as the only other possibility (Fig. 2). Once the connectivities of the four disulphides had been determined in this way, a final set of structures was calculated using DYANA and X-PLOR.

3.3. Structure analysis and description

The structural statistics for the 20 best structures of RBX (Table 1) show that the structures are well-defined and have good stereochemistry. Analysis of the structures in PROCHECK_NMR [24] shows that 92% of the residues have $\phi-\psi$ values in the allowed regions of a Ramachandran plot. Three residues, Arg^5, Gly^9 and Ile^{35}, have well-defined positive ϕ angles. The angular order parameters (S) [25,26] of the final 20 structures indicate that residues 1–2, 5–10, 13–21 and 29–39 are well defined locally, with $S > 0.8$ for both ϕ and ψ angles (Fig. 3C,D). The backbone RMSD from the mean structure is plotted as a function of residue number in Fig. 3B, which shows that the structure is well defined over most of the molecule except for residues 23–27, 35, 36 and 39–42. For the purposes of global superimposition we refer to residues 1–22 and 29–38 as being well defined (mean pairwise RMSD of 0.71 Å over the backbone heavy atoms) but in fact the whole molecule superimposes quite well.

The overall structure of RBX is depicted in Fig. 4, where the backbone heavy atoms of the 20 best structures have been superimposed over the whole molecule. The structure consists of a small triple-stranded β-sheet stabilised by a disulphide knot, followed by a C-terminal extension comprising three classic or inverse γ-turns. The disulphide knot is comprised of a ring consisting of two disulphide bonds (1–15 and 8–20) and the connecting backbone, through which a third disulphide bond (14–31) passes.

The β-sheet, defined on the basis of inter-sheet hydrogen bonds, consists of residues 6–8 (strand I), 19–21 (strand II) and 29–32 (strand III), with a topology of $+2x$, -1 (Fig. 4). The two hydrogen bonds (one amide of which has a slowly

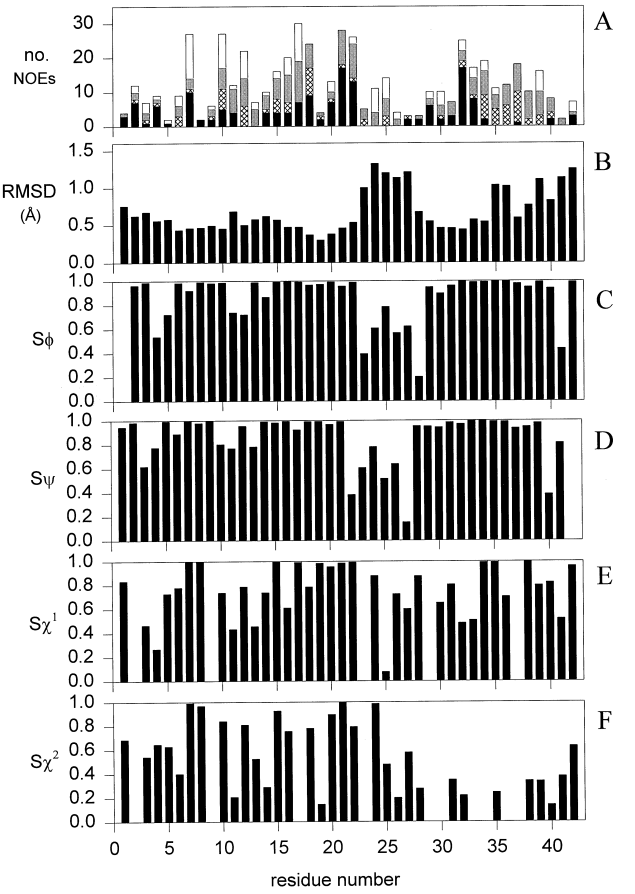

Fig. 3. Parameters characterising the final 20 structures of RBX in water at pH 5.0 and 3°C, plotted as a function of residue number. A: Upper-bound distance restraints used in the final round of structure refinement; long-range ($i-j \geq 5$), medium-range ($2 \leq i-j \leq 4$), sequential and intra-residue NOEs are shown respectively in black, cross-hatched, grey and white. NOEs are counted twice, once for each proton involved. B: RMS deviations from the mean structure for the backbone heavy atoms (N, C^{α}, C) following superposition over the whole molecule. C–F: Angular order parameters (S) [25,26] for the backbone (ϕ and ψ) and side-chain (χ^1 and χ^2) dihedral angles. Gaps in the χ^1 plot are due to Gly and Ala residues. Gaps in the χ^2 plot, in addition to Gly and Ala, are due to Ser, Pro and Thr residues.

Table 1
Structural statistics for the 20 energy-minimised structures of RBX from X-PLOR

RMS deviations from experimental distance restraints Å (320)[a]		0.028 ± 0.002
RMS deviations from experimental dihedral restraints (deg) (20)[a]		0.43 ± 0.25
RMS deviations from idealised geometry		
bonds (Å)		0.0117 ± 0.0004
angles (deg)		2.76 ± 0.05
impropers (deg)		0.40 ± 0.03
Energies (kcallmol)		
E_{NOE}		13.6 ± 1.8
E_{cdih}		0.29 ± 0.33
E_{L-J}		−119 ± 5
$E_{bond}+E_{angle}+E_{improper}$		146 ± 5
E_{elec}		−578 ± 37
Mean pairwise RMSD (Å)		
	Backbone heavy atoms	All heavy atoms
Residues 1–42	1.06 ± 0.21	1.92 ± 0.24
Residues 1–22, 29–38	0.71 ± 0.21	1.46 ± 0.27
Residues 1–22, 29–42	0.87 ± 0.23	1.66 ± 0.27
Residues 23–28	0.87 ± 0.25	2.20 ± 0.59
C-terminus (39–42)	0.68 ± 0.26	1.83 ± 0.38

[a]The numbers of restraints are shown in parentheses. None of the structures had distance violations > 0.3 Å or dihedral angle violations > 5°.

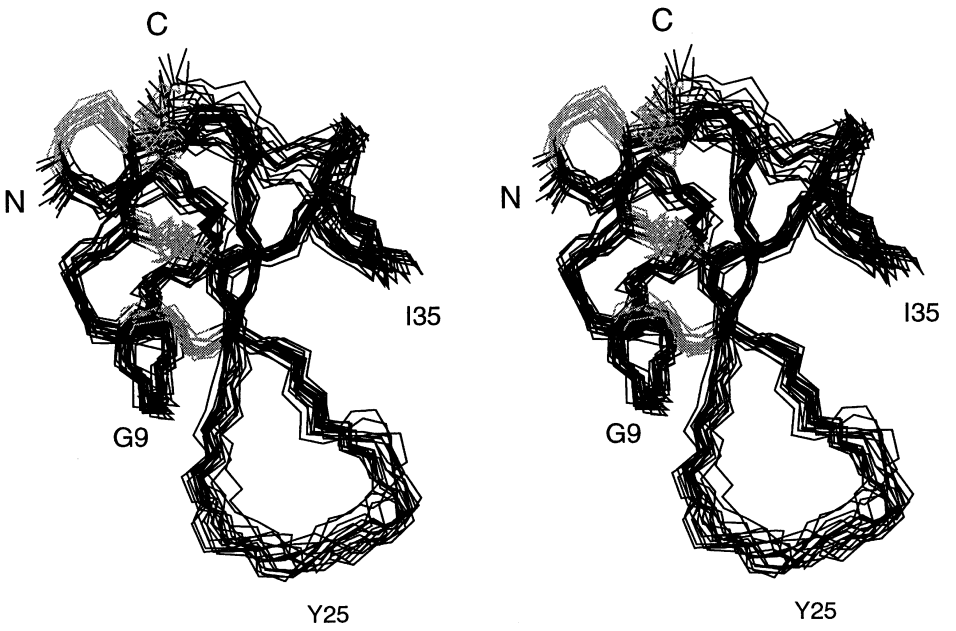

Fig. 4. Stereo view of the backbone heavy atoms and disulphide bonds of the final 20 structures of RBX in water, superimposed over the backbone heavy atoms (N, C^{α}, C) of the whole molecule. The four disulphide bonds are shown in light shading.

exchanging amide proton) between strands I and III are distorted (NH to CO distance between 2.5 and 3.0 Å). There are four hydrogen bonds between strands II and III (all of which have corresponding slowly exchanging amide protons), three being present in most of the structures and one in half of the structures.

The structure contains a number of chain reversals. The first is not well defined and is either a type II β-turn (Lys^3–Asn^6) or a γ-turn centred on Arg^5 [27]. Chain reversal II is a γ-turn centred on Gly^9. Chain reversal III is not well defined, being either a type I β-turn (Asn^{11}–Cys^{14}) or an inverse γ-turn centred on Asn^{11}. Chain reversal IV (Cys^{15}–Met^{18}) is not stabilised by a hydrogen bond but has a *cis* peptide bond between Cys^{16} and Pro^{17} and resembles a type VIa turn. The fifth chain reversal occurs in the region of residues 22–28, which fulfil the criteria for an Ω-loop [28]. The C-terminal extension, stabilised by the Cys^{16}–Cys^{42} disulphide bond, consists of three γ-turns, VI–VIII, that are, respectively, an inverse turn, centred on Thr^{33}, a classic turn centred on Ile^{35} and an inverse turn centred on Phe^{39}. All three of the γ-turn hydrogen bonds have slowly exchanging amide protons (although this is not the case for the other turns). The only slowly exchanging amide proton not accounted for by consensus hydrogen bonds in any secondary structure element is that of Gly^{37} (which hydrogen bonds to Thr^{34} in one of the structures).

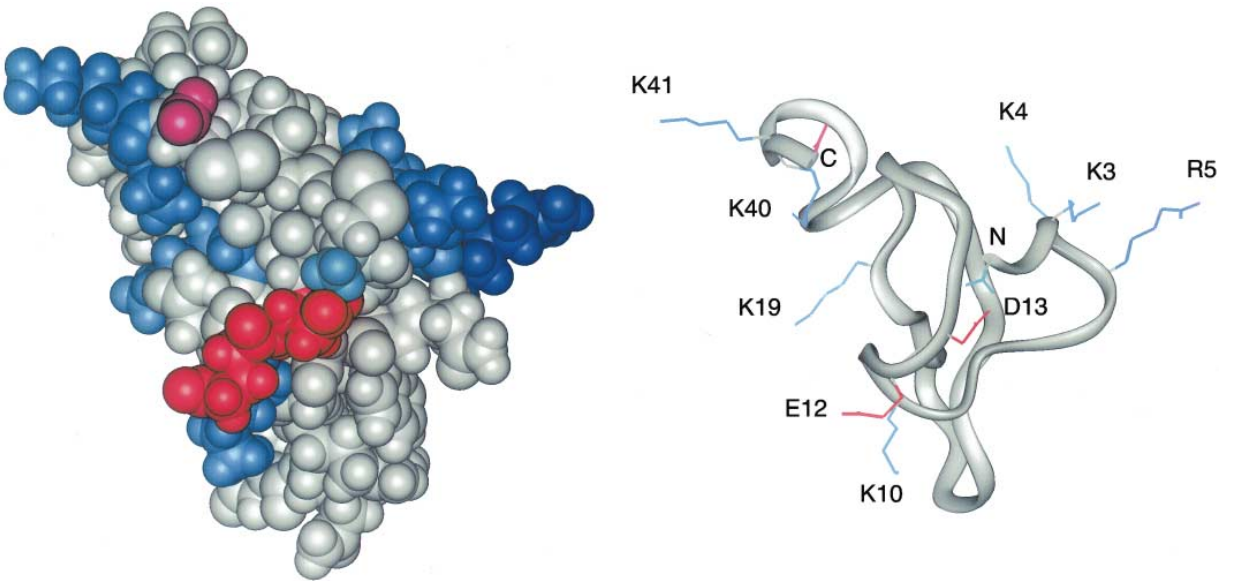

Fig. 5. Two representations of the structure of RBX closest to the average over the family of 20, highlighting the three patches of charged groups on the surface. Arg^5 is shown in dark blue, Lys in light blue, the N-terminus in cyan, Glu^{12} and Asp^{13} in red and the C-terminus in magenta. The same molecular orientation is shown in both views. This diagram was generated using Insight II.

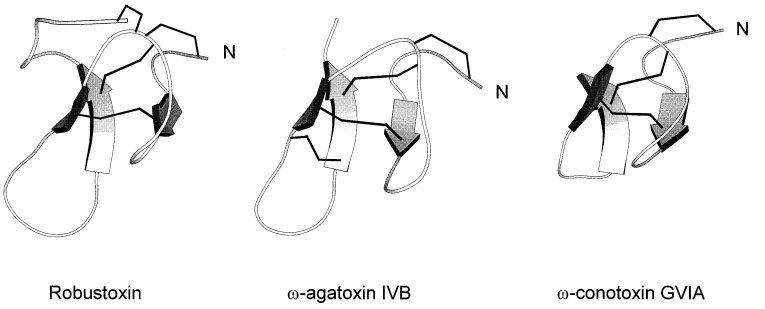

Fig. 6. Ribbon diagrams of RBX, ω-agatoxin IVB [30] and a refined solution structure of ω-conotoxin GVIA (PKP and RSN, to be published). Note that the size of the Ω-loop in RBX is the same as the corresponding loop in ω-agatoxin IVB, and they superimpose very well. The structure of ω-agatoxin IVB lacks the first three and last 10 residues, which were disordered in solution [30]. In RBX the C-terminal tail is stabilised by the 16–42 disulphide bond. This diagram was generated using MOLSCRIPT [31].

The conformations of the Cys^{1}–Cys^{15} and Cys^{8}–Cys^{20} disulphide bonds are well defined and have negative and positive χ_{SS}, respectively; the other two bonds have lower order parameters. The hydrophobic core of RBX is limited, consisting of essentially the disulphide knot cystine residues and the buried Met^{18}. However, the 22–28 loop contains one apolar residue, Ala^{23}, and three aromatics, Tyr^{22}, Trp^{24} and Tyr^{25}, and is flanked by Ile^{21} at its N-terminus and Trp^{7} near its C-terminus, so this region represents a significant non-polar surface on the molecule.

RBX is highly positively charged, with one Arg (sequence position 5) and six Lys (3, 4, 10, 19, 40 and 41) residues, balanced only by Glu^{12} and Asp^{13}. These charged residues form three patches on the surface (Fig. 5). Patch A consists of the positively charged residues 3,4 and 5, patch B of residues 10, 12, 13 and the N-terminus (including possible salt bridges between Lys^{10} and Glu^{12} and Asp^{13} and the N-terminus), and patch C of 19, 40, 41 and the C-terminus. The hydrophobic surface referred to above is on the opposite face of the molecule from that shown in Fig. 5.

3.4. Structural motif

The structure of RBX is similar to those of a family of proteins containing a small triple-stranded β-sheet and a cystine knot (the 'inhibitor cystine knot' motif) [29], as illustrated in Fig. 6. For example, the backbone RMSD between the average RBX structure and the average ω-conotoxin GVIA structure (from *Conus geographus*, a venomous cone shell) over the region of the β-sheet is 1.34 Å, while the corresponding value for the spider toxin ω-agatoxin IVB [30] is 1.02 Å. Furthermore, the positions of the half-cystines in the β-strands of RBX match precisely those expected for the motif [29].

4. Discussion

Defining the solution structure of RBX presented a considerable challenge for two reasons. First, the locations of the four disulphide bonds were not known chemically, so they had to be determined from the NMR data, a task complicated by the presence of a triplet of half-cystines at positions 14–16. Structure calculations without disulphide connectivities showed that the most likely connectivities (based on C^{β}–C^{β} and S–S distances) were 1–15, 8–20, 14–31 and 16–42 (a 1–4/2–6/3–7/5–8 pattern). An NOE from $C^{\alpha}H$ of C16 to $C^{\beta}H$ of C42 confirmed this connectivity [32] and a preliminary chemical determination of the disulphides confirmed the 1–15 and 8–20 connectivities (D.A. and P.F.A., unpublished results). Moreover, the connectivities were consistent with the 1–4/2–5/3–6 pattern expected for the conotoxin motif but with the inclusion of an additional bond linking the fifth and eighth half-cystines.

The second, and more significant, factor was that this polypeptide appeared to undergo conformational averaging in solution, which had the effect of broadening several of the backbone amide resonances and weakening or in some cases abolishing their expected NOESY cross-peaks. This significantly hampered the task of making specific resonance assignments and led to the use of a temperature of 3°C for structure determination. At this temperature several amide resonances sharpened significantly, allowing NOE connectivities to be observed, but some were still weak and had no structurally useful NOE connectivities, most notably those from residues in the 22–28 loop. The penalty paid for using such a low temperature was that several side-chain resonances were now broadened to the point where it was difficult to determine coupling constants from anti-phase cross-peaks in DQF-COSY and E-COSY spectra. As a result, there were fewer stereospecific assignments and side-chain dihedral restraints than would normally be obtained for a molecule of this size.

The structure of RBX clearly places it in the same structural class as the ω-conotoxins, various protease inhibitors and a range of other toxins and plant proteins, all of which contain a small, three-stranded, anti-parallel β-sheet and a disulphide knot [29]. This structural motif appears to be quite robust, with members of this family having little or no sequence similarity. Indeed, the defining characteristic of this structural motif at the amino acid sequence level appears to be the size of the gaps between the six key half-cystine residues, which were suggested to be $CX_{3-7}CX_{4-6}CX_{0-5}CX_{1-4}CX_{4-10}C$ [29]. The predictive value of this description has been verified by the fact that of three small proteins predicted to adopt this fold [29], all three (gurmarin [33], huwentoxin-I [34] and the AVR9 elicitor protein [35]) have since been confirmed as having this structure. Recently, the structure of an insecticidal toxin from another Australian funnel-web spider was also found to adopt this fold [36], although the first strand of the β-sheet was reduced to one residue. This toxin has a larger gap between the last two half-cystines than other members of this structural family, indicating that the definition should be expanded to $CX_{3-7}CX_{4-6}CX_{0-5}CX_{1-4}CX_{4-13}C$. Our structure for RBX

confirms that toxins with four disulphides can adopt this fold, as noted previously [29], but in the case of ω-agatoxins IVA and IVB [30,37] the fourth disulphide was located within one of the loops, whereas in RBX it connects one of the loops to the C-terminus. It is clear that this structural motif provides a robust and versatile scaffold for the presentation of a variety of functional groups, thereby generating a range of polypeptides with diverse biological targets.

The molecular target of versutoxin, a close homologue of RBX, appears to be the voltage-gated sodium channel [8]. Moreover, there are some similarities between the effects of versutoxin on the gating and kinetics of the tetrodotoxin-sensitive sodium channel and those of sea anemone toxins and scorpion α-toxins. Although further work is required to establish whether the binding sites on the sodium channel are the same and to define the channel sub-type specificities of each of these toxins, there may prove to be some similarities in how they bind to the channel. In the sea anemone and scorpion toxins, combinations of charged (especially cationic) and hydrophobic side-chains are important for binding to their receptor site (site 3) on the channel [9,38], and it will not be surprising to find that the same applies to RBX and versutoxin. In this context, it is noteworthy that RBX presents three distinct charged patches on its surface, as well as a non-polar region centred on the 22–28 loop. Further studies of RBX must now be directed towards defining which residues are important for interaction with the sodium channel so that a plausible model can be constructed of its binding site. If RBX does indeed bind to site 3 on the channel [39], then it represents a useful new scaffold, complementary to those of the sea anemone and scorpion toxins, for mapping the dimensions of this site.

Acknowledgements: We thank Dr David Sheumack for the provision of crude venom and John MacFarlane for assistance with computing.

References

[1] Gray, M.R. and Sutherland, S.K. (1978) in: Arthropod Venoms. Handbook of Experimental Pharmacology (Bettini, S., Ed.), pp. 121–148, Springer-Verlag, Berlin.
[2] Wiener, S. (1961) Med. J. Aust. 2, 693–699.
[3] Sheumack, D.D., Carroll, P.R., Hampson, F., Howden, M.E.H., Inglis, A.S., Roxburgh, C.M., Skotulis, A. and Strike, P.M. (1983) Toxicon, Suppl. 3, 397–400.
[4] Mylecharane, E.J., Spence, I., Sheumack, D.D., Claassens, R. and Howden, M.E.H. (1989) Toxicon 27, 481–492.
[5] Sutherland, S.K. (1980) in: Australian Animal Toxins, pp. 255–298, Oxford University Press, Melbourne.
[6] Sutherland, S.K. (1980) Med. J. Aust. 2, 437–441.
[7] Sheumack, D.D., Claassens, R., Whiteley, N.M. and Howden, M.E.H. (1985) FEBS Lett. 181, 154–156.
[8] Nicholson, G.M., Willow, M., Howden, M.E.H. and Narahashi, T. (1994) Pflügers Arch. 428, 400–409.
[9] Norton, R.S. (1991) Toxicon 29, 1051–1084.
[10] Couraud, F., Jover, E., Dubois, J.M. and Rochat, H. (1982) Toxicon 20, 9–16.
[11] Marion, D. and Wüthrich, K. (1983) Biochem. Biophys. Res. Commun. 113, 967–974.
[12] Sklenar, V., Piotto, M., Leppik, R. and Saudek, V. (1993) J. Magn. Reson. Ser. A 102, 241–245.
[13] Kumar, A., Ernst, R.R. and Wüthrich, K. (1980) Biochem. Biophys. Res. Commun. 95, 1–6.
[14] Macura, S., Huang, Y., Suter, D. and Ernst, R.R. (1981) J. Magn. Reson. 43, 259–281.
[15] Braunschweiler, L. and Ernst, R.R. (1983) J. Magn. Reson. 53, 521–528.
[16] Rucker, S.P. and Shaka, A.J. (1989) Mol. Phys. 68, 509–517.
[17] Rance, M., Sørensen, O.W., Bodenhausen, G., Wagner, G., Ernst, R.R. and Wüthrich, K. (1983) Biochem. Biophys. Res. Commun. 117, 479–485.
[18] Griesinger, C., Sørensen, O.W. and Ernst, R.R. (1987) J. Magn. Reson. 75, 474–492.
[19] Manoleras, N. and Norton, R.S. (1994) Biochemistry 33, 11051–11061.
[20] Montelione, G.T., Arnold, E., Meinwald, Y.C., Stimson, E.R., Denton, J.B., Huang, S.-G., Clardy, J. and Scheraga, H.A. (1984) J. Am. Chem. Soc. 106, 7946–7958.
[21] Güntert, P., Mumenthaler, C. and Wüthrich, K. (1997) J. Mol. Biol. 273, 283–298.
[22] Brunger, A.T. (1992) X-PLOR Version 3.85. A System for X-ray Crystallography and NMR, Yale University, New Haven, CT.
[23] Barnham, K.J., Dyke, T.R., Kem, W.R. and Norton, R.S. (1997) J. Mol. Biol. 268, 886–902.
[24] Laskowski, R.A., Rullmann, J.A.C., MacArthur, M.W., Kaptein, R. and Thornton, J.M. (1996) J. Biomol. NMR 8, 477–486.
[25] Hyberts, S.G., Goldberg, M.S., Havel, T.F. and Wagner, G. (1992) Protein Sci. 1, 736–775.
[26] Pallaghy, P.K., Duggan, B.M., Pennington, M.W. and Norton, R.S. (1993) J. Mol. Biol. 234, 405–420.
[27] Smith, J.A. and Pease, L.G. (1980) CRC Crit. Rev. Biochem. 8, 315–399.
[28] Leszczynski, J.F. and Rose, G.D. (1986) Science 234, 849–855.
[29] Pallaghy, P.K., Neilsen, K.J., Craik, D.J. and Norton, R.S. (1993) Protein Sci. 3, 1833–1839.
[30] Yu, H., Rosen, M.K., Saccomano, N.A., Phillips, D., Volkmann, R.A. and Schreiber, S.L. (1993) Biochemistry 32, 13123–13129.
[31] Kraulis, P. (1991) J. Appl. Crystallogr. 24, 946–950.
[32] Klaus, W., Broger, C., Gerber, P. and Senn, H. (1993) J. Mol. Biol. 232, 897–906.
[33] Arai, K., Ishima, R., Morikawa, S., Miyasaka, A., Imoto, T., Yoshimura, S., Aimoto, S. and Akasaka, K. (1995) J. Biomol. NMR 5, 297–305.
[34] Qu, Y.X., Liang, S.P., Ding, J.Z., Liu, X.C., Zhang, R.J. and Gu, X.C. (1997) J. Protein Chem. 16, 565–574.
[35] Vervoort, J., van den Hooven, H.W., Berg, A., Vossen, P., Vogelsang, R., Joosten, M.H.A.J. and de Wit, P.J.G.M. (1997) FEBS Lett. 404, 153–158.
[36] Fletcher, J.I., Smith, R., O'Donoghue, S.I., Nilges, M., Connor, M., Howden, M.E.H., Christie, M.J. and King, G.F. (1997) Nature Struct. Biol. 4, 559–566.
[37] Kim, J.I., Konishi, S., Iwai, H., Kohno, T., Gouda, H., Shimada, I., Sato, K. and Arata, Y. (1995) J. Mol. Biol. 250, 659–671.
[38] Dias-Kadambi, B.L., Drum, C.L., Hanck, D.A. and Blumenthal, K.M. (1996) J. Biol. Chem. 271, 9422–9428.
[39] Rogers, J.C., Qu, Y., Tanada, T.N., Scheuer, T. and Catterall, W.A. (1996) J. Biol. Chem. 271, 15950–15962.